Blunt Trailing Edge Profiled Body Wake Control Using Synthetic Jets

Ross Cruikshank & Philippe Lavoie

Institute for Aerospace Studies
University of Toronto
4925 Dufferin St., Toronto, Ontario, M3H 5T6, Canada
ross.cruikshank@mail.utoronto.ca & lavoie@utias.utoronto.ca

INTRODUCTION

The flow over bluff bodies is an important area of research in fluid dynamics due to its many scientific and engineering applications. Bluff body wakes involve the interaction of separated shear layers, forming a system of antisymmetric vortices (i.e., a vortex street). The distance downstream of a body that a vortex street forms is determined by the energy of the separated shear layers and the entrainment demands of the von Karman vortices. A strong vortex street leads to highly bent shear layers and a short region of recirculating flow, resulting in low pressure, high drag, and undesirable periodic aerodynamic forces. Control of the wake by affecting the entrainment balance of the shear layers can attenuate vortex shedding and reduce the pressure drag. Different control methodologies to accomplish this goal have been studied with varying degrees of success. Examples of such techniques include inhibiting shear layer interaction with a splitter plate (Bearman, 1965), opposition control of the vortex street (Siegel *et al.*, 2003), and synchronizing the roll up of the upper and lower separated shear layers to prevent asymmetry and decouple the wake and shear layers (Pastoor *et al.*, 2008). In recent years, the three-dimensional spanwise features of wakes have received increased attention due to the contribution they also make to drag and the transition of the wake to turbulence. This has motivated control techniques that involve introducing spanwise variable disturbances into the wake to induce vortex dislocations, a strategy often referred to as distributed forcing. The presence of dislocations is associated with higher base pressure and lower fluctuating aerodynamic forces, and is therefore desirable for drag reduction (Williamson, 1989).

Distributed forcing was pioneered as a passive flow control technique by Tombazis and Bearman (1997), who observed cellular shedding patterns in the wake of a bluff body outfitted with a spanwise wavy trailing edge, leading to a 34% increase in base pressure at $Re_d = 40{,}000$. As an active flow control technique, distributed forcing was first investigated by Kim and Choi (2005) with spanwise sinusoidal blowing and suction on a cylinder, and resulted in a 25% drag reduction at Reynolds numbers (Re_d) up to 3,900. Naghib-Lahouti *et al.* (2015) performed distributed forcing on a BTE body with a discrete number of plasma actuators spaced at $2.4d$ on the upper and lower surfaces and observed an increase of 40% in the base pressure at $Re_d = 3{,}000$. The spanwise spacing of $2.4d$ was selected to match a dominant cellular shedding wavelength observed in BTE body wakes at this Re_d (Naghib-Lahouti *et al.*, 2014). The present study investigates a new distributed forcing system for a BTE body using an array of synthetic jet actuators.

A large number of studies have investigated unsteady forcing to control vortex shedding, with the effects strongly dependent on the excitation frequency and the symmetry/arrangement of actuation (Colonius and Williams, 2011). Low-frequency forcing (near the shedding frequency) has the potential to directly interact with the large-scale wake structures, but can amplify fluctuations in the shear layer and wake, leading to increased drag (Barros *et al.*, 2016). In contrast, high-frequency forcing (typically an order of magnitude greater than the dominant unstable frequencies of the base flow) has been shown to increase the turbulent dissipation rate in shear layers, and consequently, decrease the turbulent kinetic energy (TKE) (e.g., Wiltse and Glezer, 1998, Cain *et al.*, 2001). In the context of bluff body wake control, high-frequency forcing has been applied to lower the entrainment, modify the shape of the mean recirculation region of the wake, and recover base pressure by 35% (Oxlade *et al.*, 2015). The mechanism of control was attributed to increased dissipation in the shear layer, which amplified the energy of the small-scales of the flow and attenuated the large-scales by enhancing the energy cascade from large to small scales. This is consistent with the results of Vukasinovic *et al.* (2010), who introduced a high-frequency jet in a flow upstream of a step, and demonstrated significant modifications to the small and large scale structures of the flow downstream of actuation. In particular, they observed an initial increase in the turbulent kinetic energy (TKE) production and in the energy contained by small-scale structures, which was then followed by a general reduction of TKE farther downstream. Therefore, unsteady high-frequency forcing is applied in the present study to attenuate vortex shedding by controlling the shear layers and separating boundary layer fluid feeding the vortex street without amplifying the low-frequency shedding instability of the flow. The experimental design for this study is provided in the next section, followed by a presentation and discussion of the results of the study, and finally a summary of the principal findings.

EXPERIMENTAL SETUP

Measurements were made in the low turbulence intensity closed-loop wind tunnel at UTIAS (Hearst and Lavoie, 2014). The Re_d of interest in the present study are 2,500, 5,000 and 10,000. The BTE body used for the experiments has a thickness, d, of 25.4 mm, a span of $26.8d$, a leading edge radius of $2.5d$, and a chord length of $12.9d$. The boundary layer was tripped by a strip of zigzag tape of 10 mm width and 0.5 mm height placed along the span on both sides of the body $2.5d$ downstream of the leading edge. Previous experiments of a model with this geometry indicated that the boundary layer becomes fully turbulent at approximately $Re_d = 9{,}000$ (Naghib-Lahouti *et al.*, 2014).

The synthetic jets employed to control the flow are composed of piezoelectric actuators clamped inside of cavities. The jets feature rectangular slot exits with lengths of $1.2d$ and aspect ratios of 38, and can be oriented streamwise and spanwise relative to the crossflow. The actuators were installed on both sides of the BTE body $1.05d$ upstream of the trailing edge, and were spaced apart by $2.4d$. A fixed forcing frequency of 2000 Hz was investigated to align with the resonance frequency of the actuator, which is an order of magnitude above the shedding and shear layer instability frequencies. The non-dimensional forcing frequency, based on the Strouhal number, $St = fd/u_\infty$, varied from 33.5 to 8.5 over the Re_d investigated. The velocity of each jet was individually calibrated with a single hot-wire placed 1 mm inside the slot such that velocity in the expulsion stroke was slightly greater than the velocity in

the suction stroke. The forcing amplitude of the synthetic jets was characterized using the velocity ratio (VR), defined as

$$\mathrm{VR} = \frac{\frac{1}{T/2}\int_0^{T/2} u_j(t)\mathrm{d}t}{u_\infty} \tag{1}$$

where T is the cycle period, $u_j(t)$ is the jet velocity, and the integration is performed over the expulsion stroke. The forcing velocities tested range from 6 to 16 m/s, producing VR from 1 to 10.7.

The effect of forcing on the wake was examined from the mean base pressure, and the wake velocity measured by two spanwise separated single hot-wires as well as PIV in multiple vertical (x-y) planes. The hot-wire array was positioned in the flow using a traverse system, and was always oriented to measure the streamwise velocity. Due to space constraints, the present discussion will focus only on velocity measurements in planes directly downstream of a jet and spanwise offset by $1.2d$ in between the jets.

A pitot-static probe placed in the freestream was used to set the freestream velocity and to determine the reference velocities for calibrating the hot-wire. It was connected to a MKS Baratron 120AD 10 Torr pressure transducer. Mean base pressure measurements were made only when the jets were oriented spanwise using a series of static pressure taps located along the base between the jets, which were connected to a MKS 225AD 1 Torr pressure transducer. A Dantec Type 55H probe and a Dantec 56C constant temperature anemometer were used for the hot-wire measurements. Hot-wire data was acquired at a sampling frequency of 25 kHz for a duration of 120 s. PIV measurements were acquired from two Lavision sCMOS cameras. The first camera had a viewing area that ranged from $x/d = [0.2, 5.75]$ and $y/d = [-2.5, 2.5]$, with a spatial resolution of $0.035d$. The second camera had a zoomed-in field of view located in the vortex formation region at $x/d = [0.15, 1.9]$ and $y/d = [-0.7, 0.7]$, with a spatial resolution of $0.01d$. The arrangement of the PIV measurement planes and the reference coordinate system is shown in Figure 1. Ensembles of 3120 random snapshots, acquired at a frequency of 2.5 Hz, were used to compute the statistics of the flow field. The raw particle images were processed by a multi-pass cross-correlation method built into DaVis software, set with 32×32 pixel interrogation windows and 50% overlap.

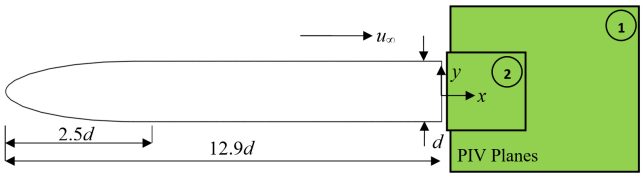

Figure 1: Schematic of the blunt trailing edge model used for the experiments, and the two PIV x-y planes. The coordinate system adopted in this study is indicated on the figure.

RESULTS AND DISCUSSION

I. Mean Base Pressure

Base pressure measurements were used to quantify the effectiveness of forcing at different amplitudes in controlling the wake, due to the close association between the base pressure and the flow in the near wake and the resulting pressure drag. The mean base pressure, referenced to the freestream static pressure of the pitot-static probe, p_∞, was calculated as

$$C_p = \frac{p - p_\infty}{\frac{1}{2}\rho u_\infty^2} \tag{2}$$

using the freestream dynamic pressure for normalization. The recovery of base pressure with forcing ($C_{p,f}$) is indicated as ΔC_p, defined as the ratio of the change in base pressure from the unforced case ($C_{p,o}$) to the unforced base pressure: $\Delta C_p = (C_{p,o} - C_{p,f})/C_{p,o}$. The effect of the forcing amplitude on ΔC_p at $Re_d = 2{,}500$, 5,000 and 10,000 is presented in Figure 2. A positive ΔC_p corresponds to a recovery of base pressure. For low VR, evident in the $Re_d = 5{,}000$ and 10,000 cases, negative pressure recovery was measured, indicating an increase in the drag and suggesting that the vortex street was strengthened. As the VR was increased, ΔC_p increased to a maximum of about 30% at a VR of 7.5 for the $Re_d = 2{,}500$ case. For the $Re_d = 5{,}000$ case, a lower maximum ΔC_p of about 20% was observed at a VR of 3.75. These results are comparable to other studies involving distributed forcing (e.g. Kim and Choi, 2005). Notably, the base pressure recovery started to decrease beyond a critical forcing amplitude for both the $Re_d = 2{,}500$ and 5,000 cases. This suggests that over forcing can lead to a reduction in the overall drag reduction. A similar result was observed by Naghib-Lahouti *et al.* (2015), who attributed this phenomena to a widening of the wake due to the forcing.

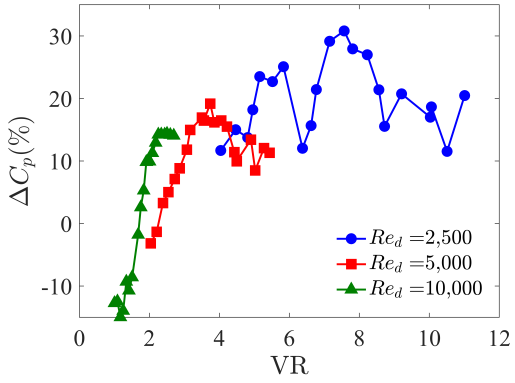

Figure 2: Mean static base pressure recovery, ΔC_p, for $Re_d = 2{,}500$, 5,000, and 10,000 with various forcing amplitudes.

II. Wake Field Effects

The PIV measurements were used to relate the changes in the base pressure due to forcing to the organization of the wake, and to gain insight into the mechanism of control. Previous investigations of slotted jets in a crossflow showed that in both spanwise and streamwise orientations, counter-rotating vortex pairs (CRVP) are produced downstream of the points of actuation (e.g. Van Buren *et al.*, 2016). An important difference between the orientations is that in the spanwise configuration, the CRVP does not penetrate as high in the boundary layer, and affects a wider region of the flow downstream.

To examine the effect of forcing on the vortex street, it is instructive to analyze the coherent large-scale features of the wake by phase-averaging based on the shedding cycle. The PIV measurements were phase-averaged using the proper orthogonal decomposition (POD) based method of van Oudheusden *et al.* (2005). In this

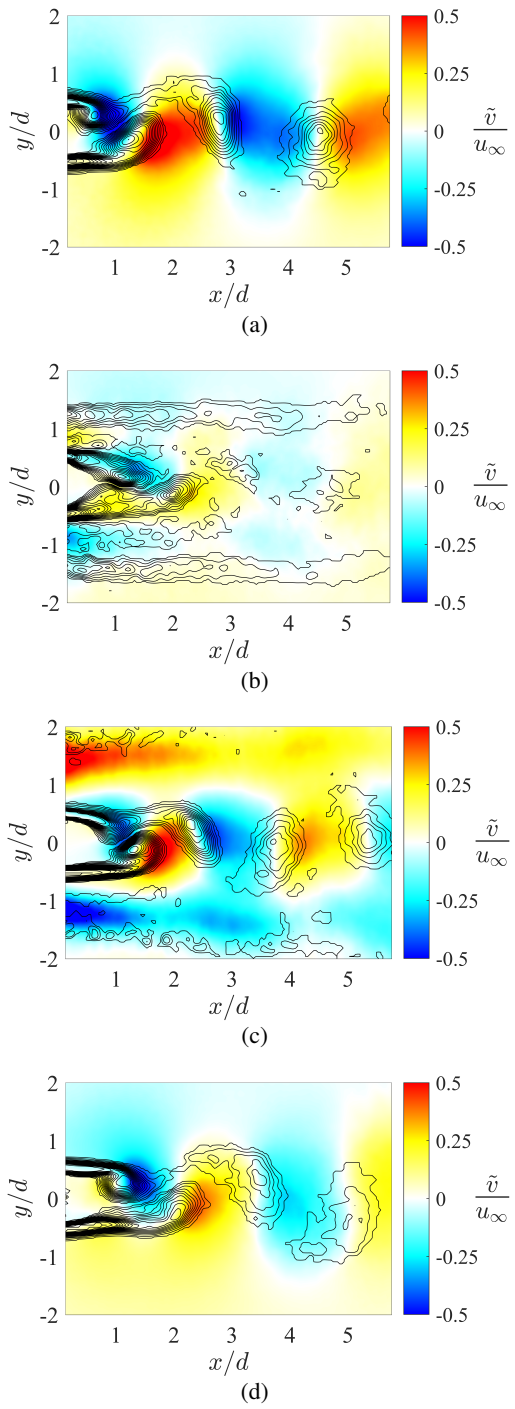

Figure 3: Phase averaged cross-stream velocity in color with superimposed isocontours of vorticity (levels separated by 0.3 $|\widetilde{\omega}d/u_\infty|$) for $Re_d = 2{,}500$ and VR = 8. **(a)** Unforced, **(b)** Spanwise array forcing downstream of a jet, **(c)** Streamwise array forcing downstream of a jet, **(d)** Spanwise array forcing spanwise offset from a jet by $1.2d$.

study, the snapshots were sorted into 18 phase bins, with roughly 170 snapshots per bin. Phase-averaged statistics are denoted as $\widetilde{s}$.

Figure 3 presents sample phase-averaged cross-stream velocity fields in color, with the isocontours of vorticity superimposed for the $Re_d = 2{,}500$ case at a VR = 8. Comparing the phase-averaged field directly downstream of a spanwise-oriented jet to the unforced case, it is clear that the von Karman vortex-induced cross-stream velocity outside the vortex formation region was substantially reduced, indicating that the vortex street was almost completely suppressed in this plane. In the vortex formation region, the cross-stream velocity surrounding the shear layers was induced by the jets and is directed away from the centerline, which is opposite to the unforced wake. In general, a vortex street grows by first entraining fluid from the log-layer of the boundary layer, and later by entraining freestream fluid (Rai, 2015). Because the fluid in the log-layer was directed away from the wake centerline with spanwise forcing, less fluid was entrained by the separated shear layers, inhibiting vortex formation. A similar mechanism occurred for streamwise forcing except that the CRVP produced by the jets penetrated higher in the boundary layer, so the initial entrainment of fluid from the log-layer was not as significantly impacted as with spanwise forcing.

With respect to the PIV measurement plane in between the jets, for which only the spanwise-oriented jet case is presented in Figure 3**d**, coherent vortex shedding is evident, in contrast to the measurement plane downstream of a jet. The considerably different structure of the wake across the span indicates the breakup of the vortex street due to the spanwise variable forcing. Despite the persistence of the vortex street in the measurement plane between the jets, the magnitude of the cross-stream velocity was reduced, which suggests the passage of weaker shed vortices.

The strength of the vortices was quantified using their circulation, Γ, calculated from the surface integral of the phase-averaged spanwise vorticity, $\widetilde{\omega}$:

$$\frac{\Gamma}{u_\infty d} = \iint_S \left(\frac{\widetilde{\omega} d}{u_\infty}\right) \frac{1}{d^2} \mathrm{d}A. \tag{3}$$

The bounds of the integration, S, were set at $|\widetilde{\omega}d/u_\infty| > 0.1$ to prevent the inclusion of relatively noisy data near the edges of the vortices. The circulation and area of the vortices when their centroid was located at $x/d = 4$ is presented in Table 1 for various VR and Re_d. This streamwise location was selected because it is well downstream of the vortex formation region, so the supply of circulation from the separated shear layers has been cut off. It can be seen that for all forcing amplitudes at $Re_d = 2{,}500$, both spanwise and streamwise forcing considerably reduced the circulation and the cross-sectional area of the von Karman vortices in the measurement plane between the jets. In particular, with spanwise forcing at a VR = 8, the circulation was reduced to about 70% of the unforced case, which is consistent with the observed reduction in the magnitude of the phase-averaged cross-stream velocity in this plane. At $Re_d = 5{,}000$, the best case scenario investigated was the streamwise orientation at a VR = 5.3, which caused the circulation to be reduced to about 85% of the unforced case. At $Re_d = 10{,}000$, the circulation was only slightly reduced for streamwise forcing (VR = 2.7), and was increased for spanwise forcing (VR = 2.3), indicating increased organization of the vortex street in between the jets. This is not unexpected given the results of the base pressure measurements, which showed that low forcing amplitudes can cause a decrease in the base pressure.

In order to better understand the effect of forcing on the initial formation of the vortex street, the mean recirculation region of the wake was analyzed with the PIV data from the zoomed-in camera. Focusing our attention on the measurement plane downstream of a jet, Figure 4 shows the mean cross-stream velocity fields in the near wake for the unforced and spanwise forced (VR = 8, $Re_d = 2{,}500$) cases. The recirculation region, given by the closing streamlines of the mean velocity field, is indicated with a solid black line. For the unforced case, the length of the recirculation region, L_f, is $1.07d$,

Table 1: Variation of the vortex circulation, Γ, and area, A, of the vortex when its centroid is located at $x/d = 4$ with Re_d, forcing amplitude (VR), and jet orientation (Span. = spanwise, Str. = streamwise) in the measurement plane spanwise offset $1.2d$ from the jets. The area is computed for $|\widetilde{\omega}d/u_\infty| > 0.1$.

Re_d	VR	$\Gamma/u_\infty d$		A/d^2	
		Span.	Str.	Span.	Str.
2,500	0	1.70		2.35	
2,500	5.3	1.45	1.45	2.10	2.20
2,500	8	1.15	1.30	2.10	1.95
2,500	9.3	1.20	1.25	1.80	1.65
2,500	10.7	—	1.20	—	1.60
5,000	0	1.60		2.30	
5,000	2.7	1.65	1.50	2.40	2.35
5,000	4	1.45	1.40	2.25	2.10
5,000	4.6	1.45	—	2.40	—
5,000	5.3	—	1.40	—	1.90
10,000	0	1.45		2.20	
10,000	2.3	1.60	—	2.60	—
10,000	2.7	—	1.40	—	2.10

whereas for the forced case it has increased to $1.22d$. The variation of length of the recirculation region for the other forcing amplitudes investigated is shown in Table 2. It may seem unusual that the maximum extent of the recirculation region was $1.67d$ at the lowest VR investigated, and decreased as the VR increased. Typically, the length of the recirculation region is considered to be inversely related to the base pressure, the velocity fluctuations in the near wake, and the entrainment rate of the vortex street. This does not hold for the present forcing scheme. A similar observation to these results was made by Oxlade *et al.* (2015) who found that with high-frequency forcing of an axisymmetric body, a positive base pressure recovery was associated with a slight shortening of the recirculation region. It was argued that this result was due to the bending of the flow streamlines near the trailing edge towards the wake centerline by the small-scale vortices created by their high-frequency jet, leading to the narrowing and shortening of the wake. In the present study, narrowing of the recirculation region with forcing can be seen in Figure 4, suggesting that a similar phenomena is present in the current experiments. Therefore, changes strictly in the length of the recirculation region cannot be related directly to the base pressure recovery and the near wake velocity fluctuations in the present study, but should instead be considered as the result of a balance between changes in the entrainment rate and flow deviation.

In order to relate the pressure and the near wake velocity field, a streamwise momentum balance around the closing streamline of the mean recirculation region was considered (Balachandar *et al.*, 1997). This can be expressed as

$$\int_C \frac{p-p_b}{\frac{1}{2}\rho u_\infty^2} n_1 \mathrm{d}s + \int_C \frac{\overline{u'u'}}{\frac{1}{2}\rho u_\infty^2} n_1 \mathrm{d}s = \int_C -\frac{\overline{u'v'}}{\frac{1}{2}\rho u_\infty^2} n_2 \mathrm{d}s \qquad (4)$$
$$[C_p] + [C_n] = [C_\tau]$$

where C is the boundary of the recirculation region, n_1 and n_2 are the unit normal direction cosines to the recirculation region boundary, p_b is the mean base pressure, and the integration is performed in the negative x-direction. The mean momentum flux through the boundary of the recirculation region can be neglected because the mean velocity is tangent to the boundary.

Table 2: Contributions of the integrated Reynolds streamwise normal and shear stresses, and estimated pressure to the streamwise momentum balance of the recirculation region in the measurement plane downstream of a jet at $Re_d = 2{,}500$.

Jet Orientation	VR	L_f	$[C_n]$	$[C_\tau]$	$[C_p]$	$\frac{\Delta[C_p]}{C_{p,o}}(\%)$
Unforced	0	1.07	0.14	0.06	-0.08	-
Spanwise	5.3	1.67	0.09	0.08	-0.02	17
Spanwise	8	1.35	0.10	0.08	-0.02	16
Spanwise	9.3	1.22	0.10	0.09	-0.01	20
Streamwise	5.3	1.31	0.13	0.08	-0.06	5
Streamwise	8	1.47	0.12	0.08	-0.03	12
Streamwise	10.7	1.37	0.11	0.09	-0.02	16

With the PIV plane data, $[C_n]$ and $[C_\tau]$ were directly calculated, and $[C_p]$ was estimated from equation 4. In this formulation, the pressure contribution, $[C_p]$, includes both the base pressure as well as the pressure along the closing streamline. Table 2 shows the effect of the forcing amplitude on the $[C_n]$, $[C_\tau]$ and $[C_p]$ contributions to the momentum balance. It can be seen that $[C_n]$ and $[C_\tau]$ are nearly equal for all the cases. For the lowest VR spanwise forcing case at a $Re_d = 2{,}500$, an initial jump in the $[C_n]$, $[C_\tau]$, and $[C_p]$ terms can be seen compared to the unforced case, and there are minimal changes to these quantities as the VR was further increased. However, as noted earlier, considerable changes in the shape of the recirculation region occur within this VR range due to the bending of the flow streamlines near the trailing edge of the body, which acts to shorten and narrow the recirculation region. In contrast, for streamwise forcing the derived $[C_p]$ contribution is observed to consistently increase with forcing amplitude over the VR investigated, and much smaller changes in the shape of the recirculation occur. The general increase in $[C_p]$ for both streamwise and spanwise forcing is consistent with the measured recovery of the mean base pressure shown in Figure 2. The change in $[C_p]$ from the unforced case, expressed relative to the mean static base pressure is included in the final column of Table 2, with values up to 20%. Recalling that the maximum overall base pressure recovery was measured to be about 30%, this implies that upwards of about one-half of the measured pressure recovery due to forcing can be attributed to changes in the fluctuating velocity in the near wake. The remainder of the base pressure recovery is likely due to the creation of a more favorable pressure gradient along the boundary of the recirculation region.

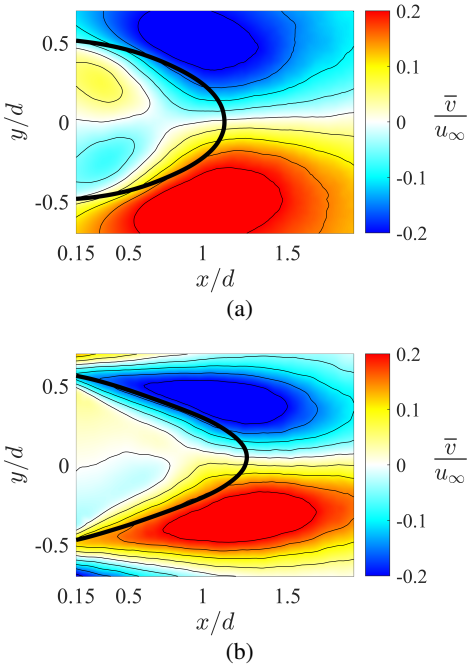

Figure 4: Mean cross-stream velocity in the wake at $Re_d = 2{,}500$, with the recirculation region shown as the thick solid line. **(a)** Unforced, **(b)** Spanwise array forcing (VR = 8) downstream of a jet.

The effect of these changes in the vortex formation region on the velocity fluctuations in the entire wake was examined from the turbulent kinetic energy (TKE), $\overline{k}$. With planar PIV, the TKE was approximated as: $\overline{k} = 0.5(\overline{u'u'} + \overline{v'v'})$. The distribution of TKE in the wake for the spanwise forcing case ($Re_d = 2{,}500$ and VR = 8) is plotted in Figure 5. In the measurement plane directly downstream of a jet, the fluctuating energy is spread over a wider width of the wake compared to the unforced case, but has a considerably reduced peak magnitude. This was also evident in the streamwise forcing case, except that the TKE induced by the jets was farther away from the wake centerline due to its CRVP penetrating higher in the boundary layer (refer also to Figure 3). Overall, the TKE in the wake was dampened to a greater extent by spanwise forcing than streamwise forcing at the same VR because the modification of the base flow with spanwise forcing occurred closer to the separated shear layers. As such, it is believed that the spanwise forcing has more of an impact on the vortex entrainment near separation. In the measurement plane between the jets, the TKE throughout the field of view is lower than the unforced case, without widening the width of the wake. This overall decrease of TKE is indicative of the ability of the controller to dampen the velocity fluctuations in the wake across the span.

A related observation from Figure 5 is that the velocity fluctuations immediately downstream of the base within the recirculation region are significantly reduced due to forcing in both the measurement planes behind and in between the jets. The magnitude of the velocity fluctuations inside the recirculation region is indicative of the amount of mixing of boundary layer fluid into the base region along the separated shear layers. Therefore, the lack of TKE in this region when forcing was applied is another indicator of reduced entrainment along the span of the body, and is consistent with the previous observations of an elongated recirculation region and the base pressure recovery.

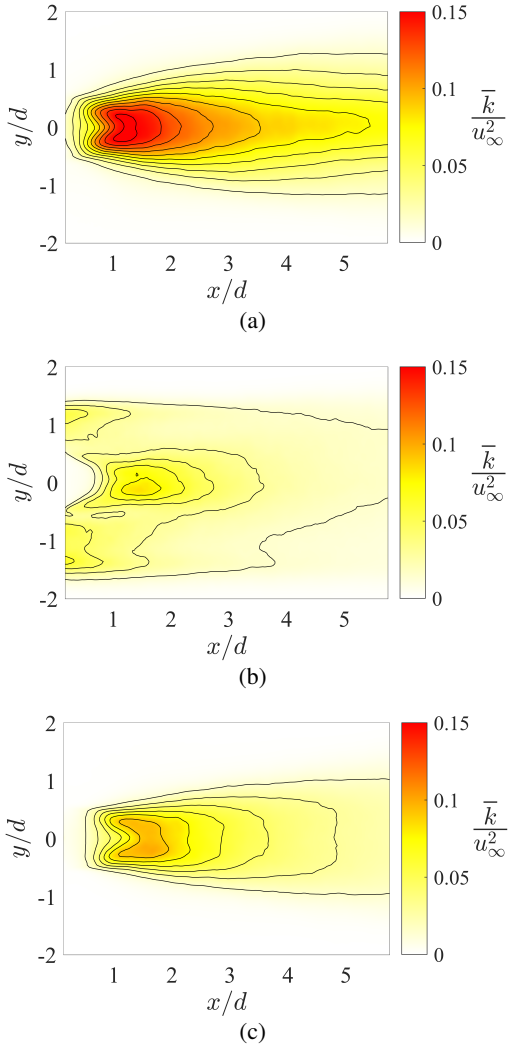

Figure 5: Turbulent kinetic energy, $\overline{k}$, for $Re_d = 2{,}500$ and VR = 8. **(a)** Unforced, **(b)** Spanwise array forcing downstream of a jet, **(c)** Spanwise array forcing spanwise offset from a jet by $1.2d$.

III. Spanwise Shedding Phase Difference

Hot-wires, spanwise separated by $1.2d$, were positioned in the separated shear layer aligned $0.25d$ downstream of the trailing edge ($y/d = 0.5$). At this position, a spectral peak at the shedding frequency was evident in both hot-wire signals, allowing the examination of the initial three-dimensional nature of the vortex street. A phase difference in the signals measured from the wires, $\Delta\theta$ (at the shedding frequency) is indicative of oblique shedding, wherein the vortex street sheds at an angle relative to the base of the body. If the phase difference crosses $[-\pi, \pi]$ it suggests the occurrence of dislocations, which are associated with momentary reductions in the near wake velocity fluctuations (Williamson, 1989). Given the spanwise periodic nature of the forcing, and the significantly different wake flow structure observed in the measurement planes downstream and spanwise offset from the jets (see Figures 3 and 5), it is expected that the forced wake will exhibit more dislocations. To compute the phase difference in the signals as a function of time, the complex Morlet transformation was used. The wrapped phase difference between the wires over a selected time interval in the unforced and spanwise forced (VR = 8) cases is presented in Figure 6**a**. It can be seen that in the forced case, crossings of $[-\pi, \pi]$ occur relatively frequently in this time segment, and do not occur

at all in the unforced case. This is due to the approximately 1.0% difference in the average shedding frequency between the two measurement points in the forced case. The reduction in the spanwise coherence of the wake is evident in the bandpass filtered (around the shedding frequency) velocity signals over the same time series (Figure 6**b**). The envelopes were computed from the analytic signal using the Hilbert transform. In the unforced case, the envelopes of the spanwise separated velocity signals have a normalized cross-covariance of about 0.55, suggesting that the vortex street is forming similarly across the span. When spanwise forcing was applied, the normalized cross-covariance of the signal envelopes was only about 0.03, indicating independence. Similar results were observed for streamwise forcing. This result demonstrates the efficacy of this flow control strategy in inducing dislocations to break the wake up into spanwise cells.

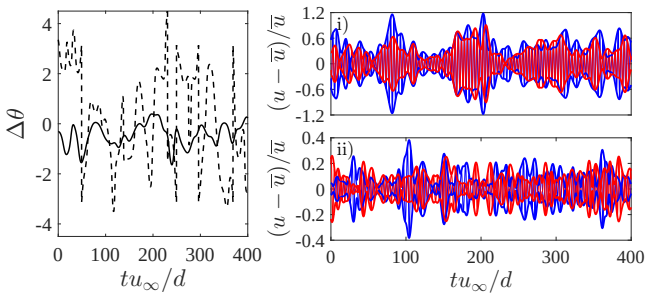

(a) (b)

Figure 6: **(a)** Wrapped phase difference between the velocity signals at the shedding frequency measured by two hot-wires spanwise separated by $1.2d$ in the shear layer $0.25d$ downstream of the trailing edge. Unforced (—), Spanwise forced at VR $= 8$ (- -).**(b)** Bandpass filtered (around the shedding frequency) velocity signals from the hot-wires, with the amplitude envelope outlined. i) Unforced, ii) Spanwise forced.

CONCLUSION

The effect of unsteady high-frequency forcing with a distributed array of streamwise and spanwise oriented synthetic jets on the wake of a blunt trailing edge profiled body was investigated at various forcing amplitudes for $2{,}500 \leq Re_d \leq 10{,}000$. Measurements of the mean base pressure showed a recovery in the base pressure up to 30% with forcing at a Re_d of 2,500 and a VR of 7.5, suggesting significant modifications in the structure of the wake. PIV, in vertical planes downstream and in between the jets, was used to quantify these changes.

It was found that in the plane downstream of the jets the vortex street could be almost completely suppressed by spanwise forcing with sufficient amplitude, leading to a corresponding drop in the TKE in the wake. These observations were attributed to the decrease in the wake entrainment due to the reduction in the velocity fluctuations in the vortex formation region and the redirection of fluid in the separated boundary layer away from the wake centerline. With streamwise forcing, the vortex street was not as significantly impacted compared to spanwise forcing because the CRVP produced by the jets penetrated higher in the boundary layer, and therefore had less influence on the separated shear layers. In the measurement plane between the jets, coherent vortex shedding was evident for both forcing orientations; however, less circulation (as low as 70% of the unforced case at VR = 8 for the spanwise orientation) was contained in the shed vortices, indicating a weaker vortex street. This is consistent with the measured base pressure recovery and reduction in the spanwise coherence of the vortex street, and demonstrates the ability of the distributed forcing technique to control the region of the wake downstream of actuation as well as between the jets.

REFERENCES

Balachandar, S., Mittal, R. & Najjar, F.M. 1997 Properties of the mean recirculation region in the wakes of two-dimensional bluff bodies. *J. Fluid Mech.* **351**, 167-199.

Barros, D., Boree, J., Noack, B. & Spohn, A. 2016 Resonances in the forced turbulent wake past a 3D blunt body. *Phys. Fluids* **28**.

Bearman, P. 1965 Investigation of the flow behind a two-dimensional model with a blunt trailing edge and fitted with splitter plates. *J. Fluid Mech.*, **21** (2), 241-255.

Cain, A., Rogers, M., Kibens, V. & Raman, G. 2001 Simulations of high-frequency excitation of a plane wake. *AIAA* **2001-0514**.

Colonius, T. & Williams, D. 2011 Control of vortex shedding on two and three-dimensional aerofoils. *Phil. Trans. R. Soc.* **369**, 1525-1539.

Hearst, R. & Lavoie, P. 2014 Decay of turbulence generated by a square-fractal-element grid. *J. Fluid Mech.*, **741**, 567-584.

Kim, J. & Choi, H. 2005 Distributed forcing of flow over a circular cylinder. *Phys. Fluids* **17**.

Naghib-Lahouti, A., Lavoie, P. & Hangan, H. 2014 Wake instabilities of a blunt trailing edge profiled body at intermediate Reynolds numbers. *Exp. Fluids*. **55**.

Naghib-Lahouti, A., Hangan, H. & Lavoie, P. 2015 Distributed forcing flow control in the wake of a blunt trailing edge profiled body using plasma actuators. *Phys. Fluids* **27**.

Oxlade, A., Morrison, J., Qubain, A. & Rigas, G. 2015 High-frequency forcing of a turbulent axisymmetric wake. *J. Fluid Mech.* **770**, 305-318.

Pastoor, M., Henning, L., Noack, B., King, R. & Tadmor, G. 2008 Feedback shear layer control for bluff body drag reduction. *J. Fluid Mech.* **608**, 161-196.

Rai, M. 2015 Detached shear-layer instability and entrainment in the wake of a flat plate with turbulent separating boundary layers. *J. Fluid Mech.* **774**, 5-36.

Siegel S., Cohen K. & McLaughlin T. 2003 Feedback control of a circular cylinder wake in experiment and simulation." *AIAA Conference*, Orlando, 2003-3569.

Tombazis, N. & Berman, P.W. 1997 A study of three-dimensional aspects of vortex shedding from a bluff body with a mild geometric disturbance. *J. Fluid Mech.* **330**, 85-112.

Van Buren, T., Leong, C., Whalen, E. & Amitay, M. 2016 Impact of orifice orientation of a finite span synthetic jet interaction with a crossflow. *Phys. Fluids* **28**.

van Oudheusen, B., Scarano, F., van Hinsberg, N.P., & Watt, D.W. 2005 Phase-resolved characterization of vortex shedding in the near wake of a square-section cylinder at incidence. *Exp. Fluids* **39**, 86-98.

Vukasinovic, B., Rusak, Z. & Glezer, A. 2010 Dissipative small-scale actuation of a turbulent shear layer. *J. Fluid Mech.* **656**, 51-81.

Williamson, C. 1989 Oblique and parallel modes of vortex shedding in the wake of a circular cylinder at low Reynolds numbers. *J. Fluid Mech.* **206**, 579-627.

Wiltse, J. & Glezer A. 1998 Direct excitation of small-scale motions in free shear flows. *Phys. Fluids* **8**, 2026-2036.